7

Numerical Simulation of Biofuels Injection

Jorge Barata and André Silva
Aerospace Sciences Department, University Beira Interior,
Covilhã,
Portugal

1. Introduction

The use of alternative biofuels in the co-generation of electricity and heat, as well as in the transportation sector, presents major benefits, such as the conservation of the environment due to their renewable origin, the reduction of fossil fuels use or the conservation of agricultural activity in regions where the food production is being reduced.

The more important biofuels currently under investigation are the bio-alchohols and their derived ethers, and the vegetable oils and their derived esters. Methyl esters of rapeseed oils or soybean oils have been tested in Diesel engines, and in spite of the strong dispersion of the published results, there are indications that their use is a promising solution to the problems originated with the raw vegetable oil due to their higher viscosity, boiling temperature, final temperature of distillation and point of obstruction of cold filter (Tinaut, 2005).

The present work presents a numerical study on evaporating biofuel droplets injected through a turbulent cross-stream. This study uses an Eulerian/Lagragian approach to account for turbulent transport, dispersion, evaporation and coupling between both processes in practical spray injection systems, which usually include air flows in the combustion chamber like swirl, tumble and squish in I.C. engines or crossflow in boilers and gas turbines. An array of evaporating biofuel droplets through a crossflow is studied, and a comparison of the droplet fuel dispersion and evaporation with conventional fuels is performed. A summary of the main general characteristics properties of the conventional fuels and biofuels tested in the present investigation is presented in Table 1.

The evaporation of droplets in a spray involves simultaneous heat and mass transfer processes in which the heat for evaporation is transferred to the drop surface by conduction and convection from the surrounding hot gas, and vapour is transferred by convection and diffusion back into the gas stream. The overall rate of evaporation depends on the pressure, temperature, and transport properties of the gas; the temperature, volatility and diameter of the drops in the spray; and the velocity of the drops relative to that of the surrounding gas (Faeth, 1983, 1989, 1986).

Godsave (1953) and Spalding (1953) gave the basic droplet vaporization/combustion model for an isolated single-component droplet in a stagnant environment. Since then this model has been studied extensively both experimentally and theoretically. These studies have been reviewed extensively by several authors during the past decades (e.g. Williams, 1973; Faeth, 1977; Lefebvre 1989; Law, 1982; and Sirignano, 1978), and are mostly dedicated to study the

dynamics of a single droplet. Abramzon and Sirignano (1989) and Berlemont et al. (1995) presented droplet vaporization models for the case of a spray in stagnant surroundings, and showed that the convective effects were most relevant. The same type of configuration was studied by Chen and Pereira (1992), and the predictions were found to follow satisfactorily the measurements presented. More recently, Sommerfeld (1998) presented a study on stationary turbulent sprays, using a droplet evaporation model based on the model proposed by Abramzon and Sirignano (1989), and revealed a general good agreement with experiments.

	n-Heptane	Rapeseed Methyl Ester (RME)	Diesel Fuel (DF-2)	Ethanol
Molecular mass, M_F	100.16	300	198	46
Fuel density at 288.6°K, $\rho_{F288.6K}$	687.8 Kg/m^3	880 Kg/m^3	846 Kg/m^3	790 Kg/m^3
Boiling temperature at atmospheric pressure, T_{bn}	371.4°K	613°K	536.4°K	351°K
Latent heat of vaporization at atmospheric pressure, L_{Tbn}	371,8KJ/Kg	254KJ/Kg	254KJ/Kg	904KJ/Kg

Table 1. Characteristic properties of biofuels compared with n-Heptane and Diesel Fuel.

If special attention is dedicated to the biofuels injection and evaporation, then practically no numerical or experimental studies can be found. Recently Bai et al. (2002) presented a most relevant numerical study of a spray in wind tunnel using the Arcoumanis et al. (1997) experiments, but concentrated on the development of the spray impingement model and the fuel used was gasoline.

2. Mathematical model

This section describes the mathematical model for turbulent particle dispersion and vaporization assuming that the particles are sufficiently dispersed so that particle-particle interaction is negligible.

The particle phase is described using a Lagrangian approach while an Eulerian frame is used to describe the effects of both interphase slip and turbulence on particle motion using random-sampling techniques (Monte Carlo). It is also assumed that the mean flow is steady and the material properties of the phases are constant.

When vaporizing droplets are involved in the simulations, two-way coupling must be accounted for since the phase change modifies the characteristics of the fluid phase. The vapour produced by the droplets is a mass source for the fluid; moreover the vaporization process generates modifications in the momentum and energy balances between both phases. Fluid phase equations then contain many extra-source terms. It is assumed that the vapour production does not significantly modify the fluid phase density.

The method to solve the continuous phase is based on the solution of the conservation equations for momentum and mass. Turbulence is modelled with the "*k*-*ε*" turbulence model of Launder and Spalding (1974), which is widely and thoroughly tested, and was found to predict reasonably well the mean flow (Barata, 1998). In order to reduce the numerical errors to an acceptable level, the higher-order QUICK scheme of Leonard (1979) is used to evaluate the convection terms. A similar method has been used for three-dimensional (Barata, 1998) or axisymmetric flows (Shuen et al., 1985; Lilley, 1976; Lockwood & Naguib, 1975) and only the main features are summarized here.

The governing equations (continuity, momentum, turbulent kinetic energy, dissipation, enthalpy, and vapour mass fraction) constitute a set of coupled partial differential equations that can be reduced to a single convective-diffusive conservation equation of the form

$$\frac{\partial(\rho U_i \phi)}{\partial X_i} = \frac{\partial}{\partial X_i}\left[\Gamma_\varphi \frac{\partial \phi}{\partial X_i}\right] + S_\varphi \tag{1}$$

where Γ_ϕ is the effective diffusion coefficient for quantity ϕ. The term on the left-hand side is the convection term, whilst the first and the second terms on the right-hand side are the diffusion term and the source term, respectively.

The source term S_ϕ as divided into two parts, which yields the following expression:

$$S_\phi = S_{\phi g} + S_{\phi p} \tag{2}$$

where $S_{\phi g}$, specifies the source term of the gas and $S_{\phi p}$, specifies the source term of the particle.

ϕ	$S_{\phi g}$	$S_{\phi p}$	Γ_ϕ
1	-	$\overline{S_{\rho,p}}$	-
U_i	$-\frac{\partial}{\partial X_i}(P+\frac{2}{3}k)-\frac{\partial}{\partial X_j}\frac{2}{3}\mu_t\frac{\partial \overline{U_j}}{\partial X_i}+\rho g_i$	$\overline{S_{U_i,p}}$	$\mu+\mu_T$
T	0	$\overline{S_{T,p}}$	$\frac{\mu}{\mathrm{Pr}}+\frac{\mu_T}{\mathrm{Pr}_T}$
Y_p	0	$\overline{S_{Y_k,p}}$	$\frac{\mu}{Sc}+\frac{\mu_T}{Sc_T}$
k	$G-\rho\varepsilon$	$\overline{S_{k,p}}$	$\mu+\frac{\mu_T}{\sigma_k}$
ε	$C_{\varepsilon 1}\frac{\varepsilon}{k}G-C_{\varepsilon 2}\rho\varepsilon$	$\overline{S_{\varepsilon,p}}$	$\mu+\frac{\mu_T}{\sigma_\varepsilon}$

Table 2. Terms in the general form of the differential equation.

The source terms of the gas phase, $S_{\phi g}$ and the effective diffusion coefficient Γ_{ϕ}, are summarized in table 2 for different depended variables. G is the usual turbulence energy production term defined as:

$$G = \mu_t \left[\frac{\partial \overline{U_i}}{\partial X_j} + \frac{\partial \overline{U_j}}{\partial X_i} \right] \frac{\partial \overline{U_i}}{\partial X_j} \tag{3}$$

and

$$\mu_t = C_\mu \rho \frac{k^2}{\varepsilon} \tag{4}$$

The turbulence model constants that are used are those indicated by Launder and Spalding (1974) that have given good results for a large number of flows, and are summarized in the next table.

$C\mu$	$C_{\varepsilon 1}$	$C_{\varepsilon 2}$	σ_k	σ_ε	$C_{\varepsilon 3}$	Pr_t	Sc_t	Pr	Sc
0.09	1.44	1.92	1.0	1.3	1.1	0.6	0.85	$\mu C_P / k_g$	$\mu / \rho D$

Table 3. Turbulence model constants.

Vaporization phenomena are described in the present study assuming spherical symmetry for heat and mass transfers between the droplet and the surrounding fluid, and convection effects are taken into account by introducing empirical correlation laws.

The main assumptions of the models are: spherical symmetry; quasi-steady gas film around the droplet; uniform physical properties of the surrounding fluid; uniform pressure around the droplet; and liquid/vapor thermal equilibrium on the droplet surface.

The effect of the convective transport caused by the droplet motion relative to the gas was a accounted for by the so called "film theory", which results in modified correlations for the Nusselt and Sherwood numbers. For rapid evaporation (i.e boiling effects) additional corrections were applied. The infinite droplet conductivity model was used to describe the liquid side heat transfer taking into account droplet heat-up. Hence, the following differential equations for the temporal changes of droplet size and temperature have to be solved.

$$\frac{dD_p}{dt} = -\frac{2\dot{m}}{\pi \rho_F D_p^2} \tag{5}$$

$$\frac{dT_p}{dt} = \frac{6Q_L}{\pi \rho_F C_{P_F} D_p^3} \tag{6}$$

Under the assumption of steady state conditions in the gas film and assuming a spherical control surface around the droplet, the total mass flow through this surface will be equal to the evaporation rate $\dot{m}$:

$$\dot{m} = \pi \overline{\rho_g D_g} D_p Sh^* \ln(1 + B_M) \tag{7}$$

and

$$\dot{m} = \pi \frac{\overline{K_{vap}}}{\overline{C_{pvap}}} D_p Nu^* \ln(1 + B_T) \tag{8}$$

the quantity $\overline{\rho_g D_g}$ can be replaced with K_{vap}/C_{pvap}, assuming a Lewis number of unity.

The heat penetrating into the droplet can be expressed by:

$$Q_L = \dot{m}\left(\frac{\overline{C_{vap}}(T_\infty - T_s)}{B_M} - L(T_s) \right) \tag{9}$$

The mass transfer number B_M as defined as

$$B_M = \frac{Y_{Fs} - Y_{F\infty}}{1 - Y_{Fs}} \tag{10}$$

where Y_{Fs} is the fuel mass fraction on the droplet surface and defined as:

$$Y_{Fs} = \left[1 + \left(\frac{P}{P_{Fs}} - 1 \right) \frac{M_A}{M_F} \right]^{-1} \tag{11}$$

For any given value of surface temperature, the vapor pressure is readily estimated from the Clausius-Claperyon equation as

$$P_{Fs} = \exp\left(a - \frac{b}{T_s - 43} \right) \tag{12}$$

where a and b are constants of the fuel.

The latent heat of vaporization is given by Watson (1931) as

$$L(T_s) = L_{tbn} \left(\frac{T_{cr} - T_s}{T_{cr} - T_{bn}} \right)^{-0.38} \tag{13}$$

Equations 7 and 8 for $\dot{m}$ are similar to the expressions for the droplet vaporization rate predicted by the classical model, with the values of the non-dimensional parameters Nu_0 and Sh_0 in the classical formulas substituted by Nu^* and Sh^* respectively. Where are expressed as

$$Sh^* = 2 + (Sh_0 - 2) / F_M \tag{14}$$

$$Nu^* = 2 + (Nu_0 - 2) / F_T \tag{15}$$

The parameters Nu^* and Sh^* are the "modified" Nusselt and Sherwood numbers, and tend to Nu_0 and Sh_0, respectively, as F_T and F_M tend to the unity.

In the case of an isothermal surface and constant physical properties of the fluid, the problem has a self-similar solution and the correction factors F_M and F_T do not depend on the local Reynolds number. It was found that the values F_M and F_T are practically insensitive to the Schmidt and Prandtl numbers and the wedge angle variations, and can be approximated as

$$F_M = F(B_M), \quad F_T = F(B_T) \tag{16}$$

where $F(B)$ is given by

$$F(B) = (1+B)^{0.7} \frac{\ln(1+B)}{B} \tag{17}$$

Nu_0 and Sh_0 are evaluated by the Frossling correlations:

$$Nu_0 = 2 + 0.552 \mathrm{Re}^{1/2} \mathrm{Pr}^{1/3} \tag{18}$$

$$Sh_0 = 2 + 0.552 \mathrm{Re}^{1/2} Sc^{1/3} \tag{19}$$

The evaporation rate $\dot{m}$ with convection is:

$$\dot{m} = \pi \overline{\rho_g D_g} D_p \ln(1+B_M) \left(2 + \frac{0.552 \mathrm{Re}^{1/2} Sc^{1/3}}{F_M} \right) \tag{20}$$

and

$$\dot{m} = \pi \frac{\overline{K_{vap}}}{\overline{C_{pvap}}} D_p \ln(1+B_T) \left(2 + \frac{0.552 \mathrm{Re}^{1/2} \mathrm{Pr}^{1/3}}{F_T} \right) \tag{21}$$

The Schmidt number and the Prandtl number are equal assuming a Lewis number of unity. Equation 20 has the advantage that it applies under all conditions, including the transient state of droplet heat-up, whereas Eq. (31) can only be used for steady-state evaporation.

Finally the evaporation rate $\dot{m}$ is:

$$\dot{m} = 2\pi \frac{\overline{K_{vap}}}{\overline{C_{pvap}}} D_p \ln(1+B_M) \left(1 + \frac{0.276 \mathrm{Re}^{1/2} \mathrm{Pr}^{1/3}}{F_M} \right) \tag{22}$$

And the equations for the temporal changes of droplet size and temperature are:

$$\frac{dD_p}{dt} = -\frac{4K_{vap}\ln(1+B_M)}{C_{pvap}\rho_F D_P}\left(1+\frac{0.276\,\mathrm{Re}^{1/2}\,\mathrm{Pr}^{1/3}}{F_M}\right) \tag{23}$$

$$\frac{dT_p}{dt} = \frac{12K_g\ln(1+B_M)}{Cv_{ap}\rho_F D_P^2 C_{P_F}}\left(1+\frac{0.276\,\mathrm{Re}^{1/2}\,\mathrm{Pr}^{1/3}}{F_M}\right)\left(\frac{C_{vap}(T_\infty - T_s)}{B_M} - L(T_s)\right) \tag{24}$$

Of the air/vapor mixture in the boundary layer near the droplet surface according to Hubbard et al. (1973), the best results are obtained using the one-third role (Sparrow & Gregg, 1958), where average properties are evaluated at the following reference temperature and composition:

$$T_r = T_s + \frac{T_\infty - T_s}{3} \tag{25}$$

$$Y_{Fr} = Y_{Fs} + \frac{Y_{F\infty} - Y_{Fs}}{3} \tag{26}$$

For example, the reference specific heat at constant pressure is obtained as

$$C_{p_{vap}} = Y_{Ar}\left(C_{p_{Ar}} \quad at \quad T_r\right) + Y_{Fr}\left(C_{p_F} \quad at \quad T_r\right) \tag{27}$$

The dispersed phase was treated using the Lagrangian reference frame. Particle trajectories were obtained by solving the particle momentum equation through the Eulerian fluid velocity field, for a sufficiently high number of trajectories to provide a representative statistics.

The equations used to calculate the position and velocity of each particle were obtained considering the usual simplification for dilute particle-laden flows (Shuen et al., 1985). Static pressure gradients are small, particles can be assumed spherical and particle collisions can be neglected. Since $\rho_p/\rho_f \rangle 200$, the effects of Basset, virtual mass, Magnus, Saffman and buoyancy forces are negligible (Arcoumanis et al., 1997; Lockwood & Naguib, 1975). In dilute flows of engineering interest, the steady-state drag term is the most important force acting on the particle. Under these conditions the simplified particle momentum equation is:

$$\frac{\partial u_{p;i}}{\partial t} = \frac{1}{\tau_p}\left(u_{f;i} - u_{p;i}\right) + g_i \tag{28}$$

The mathematical expression for the relaxation time, τ_p, is

$$\tau_p = \frac{24\rho_p D_p^2}{18\mu_f C_D\,\mathrm{Re}_p} \tag{29}$$

where Re_p is the particle Reynolds number,

$$\mathrm{Re}_p = \frac{\rho_f\left|\overrightarrow{V_p} - \overrightarrow{V_f}\right| D_p}{\mu_f} \tag{30}$$

Note that the physical properties of ρ_f and μ_f should be evaluated at the reference temperature T_r and are

$$\mu_f = Y_{Ar}\left(\mu_A \text{ at } T_r\right) + Y_{Fr}\left(\mu_F \text{ at } T_r\right) \tag{31}$$

$$\rho_{vap} = \left(\frac{Y_{Ar}}{\rho_A} + \frac{Y_{Fr}}{\rho_F}\right)^{-1} \tag{32}$$

and C_D is the drag coefficient (Shirolkar et al., 1996),

$$C_D = \left(\frac{24}{\mathrm{Re}_p}\right)\left(1 + 0.15\mathrm{Re}_p^{0.687}\right) \tag{33}$$

for Re_p<10^3.

The particle momentum equation can be analytically solved over small time steps, Δt , and the particle trajectory is given by

$$u_{p;i}^{NEW} = u_{f;i} + \left(u_{p;i}^{OLD} - u_{f;i}\right)e^{-\Delta t/\tau_p} + g_i\tau_p\left[1 - e^{-\Delta t/\tau_p}\right] \tag{34}$$

$$x_{p;i}^{NEW} = x_{p;i}^{OLD} + \frac{\Delta t}{2}\left(u_{p;i}^{NEW} + u_{p;i}^{OLD}\right) \tag{35}$$

The critical issues are to determine the instantaneous fluid velocity and the evaluation of the time, Δt, of interaction of a particle with a particular eddy.

The time step is obviously the eddy-particle interaction time, which is the minimum of the eddy lifetime, τ_{FL} , and the eddy transit time, t_c. The eddy lifetime is estimated assuming that the characteristic size of an eddy is the dissipation length scale in isotropic flow:

$$l_e = B\frac{k^{3/2}}{\varepsilon} \approx C_\mu^{3/4}\frac{k^{3/2}}{\varepsilon} \tag{36}$$

$$\tau_{FL} = A\frac{k}{\varepsilon} \approx 0.2\frac{k}{\varepsilon} \tag{37}$$

where A and B are two dependent constants (Shirolkar et al., 1996).

The transit time, t_c, is the minimum time a particle would take to cross an eddy with characteristic dimension, l_e, and is given by

$$t_c = \frac{l_e}{\left|\overrightarrow{v_d}\right|} \tag{38}$$

where $\overrightarrow{v_d}$ is the relative velocity between the particle and the fluid (drift velocity).

A different expression for the transit time is also recommended in the literature (Shitolkar et al., 1996; Shuen et al., 1983; Gosman & Ioannides, 1981), and was used in the present work:

$$t_c = -\tau_p \ln\left(1 - \frac{l_e}{\tau_p \left|u_{f;i} - u_{p;i}\right|}\right) \tag{39}$$

where the drift velocity is also estimated at the beginning of a new iteration.

This equation has no solution when $l_e > \tau_p \left|u_{f;i} - u_{p;i}\right|$, that is, when the linearized stopping distance of the particle is smaller than the eddy size. In such a case, the particle can be assumed to be trapped by the eddy, and the interaction time will be the eddy lifetime.

The instantaneous velocity at the start of a particle-eddy interaction is obtained by random sampling from an isotropic Gaussian *pdf* having standard deviations of $\sqrt{2/3k}$ and zero mean values.

The above isotropic model was extended in the present work to account for cross-correlation's and anisotropy. To obtain the fluctuating velocities u'_f and v'_f, two fluctuating velocities u'_1 and u'_2 are sampled independently, and then are correlated using the correlation coefficient R_{uv}:

$$u'_f = u'_1 \tag{40}$$

$$v'_f = R_{uv} u'_1 + \sqrt{1 - R_{uv}^2}\, u'_2 \tag{41}$$

where $R_{uv} = \dfrac{\overline{u'_f v'_f}}{\sqrt{\overline{u'^2_f}}\sqrt{\overline{v'^2_f}}}$ was obtained from the measurements.

The interaction between the continuous and dispersed phase is introduced by treating particles as sources of mass, momentum and energy to the gaseous phase. The source terms due to the particles are calculated for each Eulerian cell of the continuous phase and are summarized in Table 4, and can be divided into two parts, which yields the following expression:

$$S_{\phi p} = S_{\phi i} + S_{\phi m} \tag{42}$$

where $S_{\phi i}$ specifies the source term due to inter-phase transport and $S_{\phi m}$ takes into consideration the transfer caused by evaporation.

To represent the temporal changes of droplet size and temperature Chen and Pereira (1992) used the following equations.

$$\frac{dD_p}{dt} = -\frac{4K_{vap}}{C_{p_{vap}}} \ln\left(1 + \frac{C_{p_{vap}}}{L(T_s)}(T_\infty - T_s)\right)\left(1 + 0.23\,\mathrm{Re}^{\frac{1}{2}}\right) \tag{43}$$

$$\frac{dT_p}{dt} = 12K_g * \left(\frac{(T_\infty - T_s)}{\rho_F D_P^2 C_{P_F}}\right) * \left(1 + 0.3\,\mathrm{Re}^{1/2} * \mathrm{Pr}^{1/3}\right) \tag{44}$$

In the last equation is assumed that the prevailing mode of heat transfer is forced convection, no evaporation occurs during the preheating period and the temperature is uniform across the droplet radius. For the forced convection the Ranz and Marshall (1952) correlation has taken the place of the Nusselt Number.

The solution of the governing equations was obtained using a finite-difference method that used discretized algebraic equations deduced from the exact differential equations that they represent. In order to reduce the numerical diffusion errors to an acceptable level, the quadratic upstream-weighted interpolation scheme was used (Leonard, 1979). Nevertheless, the usual grid independence tests were performed.

$S_{\phi p}$	$S_{\phi i}$	$S_{\phi m}$
$\overline{S_{\rho,p}}$	0	$\sum_p \frac{\dot{m}_p N_p}{V_{i,j}}$
$\overline{S_{U_i,p}}$	$-\sum_p \frac{\dot{m}_p N_p}{V_{i,j}}\left[\left(u_{j,p}^{\,t+\Delta t} - u_{j,p}^{\,t}\right) - g_i \Delta t\right]$	$\sum_p \frac{\dot{m}_p N_p u_{ia}}{V_{i,j}}$
$\overline{S_{T,p}}$	$-\sum_p \frac{N_p}{V_{i,j}}\left(\frac{L_{tbn}\dot{m}_p + Q_L}{C_{P_A}}\right)$	$\sum_p \frac{\dot{m}_p N_p}{V_{i,j}}\left(\frac{C_{P_{vap}}(T_s)*(T_r - T_s)}{C_{P_A}}\right)$
$\overline{S_{Y1,p}}$	0	0
$\overline{S_{Y2,p}}$	0	$\sum_p \frac{\dot{m}_p N_p}{V_{i,j}}$
$\overline{S_{k,p}}$	$\overline{U_j S_{Uji}} - \overline{U_j}\ \ \overline{S_{Uji}}$	$\overline{U_j S_{Ujm}} - \overline{U_j}\ \ \overline{S_{Ujm}} + \frac{1}{2}\overline{U_j}\ \ \overline{U_j}\ \ \overline{S_m} - \frac{1}{2}\overline{U_j U_j S_m}$
$\overline{S_{\varepsilon,p}}$	$C_{\varepsilon 3}\frac{\varepsilon}{k}\overline{S_{ki}}$	$C_{\varepsilon 3}\frac{\varepsilon}{k}\overline{S_{km}}$

Table 4. Dispersed phase source terms.

The computational domain (see Fig. 1) has six boundaries where dependent values are specified: an inlet plane and outlet planes, a symmetry plane, and three solid walls at the top, bottom and side of the channel. At the inlet boundary, uniform profiles of all dependent variables are set, while at the outflow boundaries, the gradients of dependent variables in the perpendicular direction are set to zero. On the symmetry plane, the normal velocity vanishes, and the normal derivates of the other variables are zero. At the solid surfaces, the wall function method described in detail by Launder and Spalding (1974) is used to prescribe the boundary conditions for the velocity and turbulence quantities, assuming that the turbulence is in state of local equilibrium.

The cross section of the computational domain is 0.05 x 0.05 m, whilst the channel length is 0.273 m. The droplets injection is perpendicular to the crossflow and the location of the injection point is 0.023 m far from the inlet plane ($Z_{in}/H = 0.46$).

The monosize array of droplets of 230μm of diameter is injected with an initial velocity V_P=-1m/s and a temperature of 293K or 443K through a crossflow with W_c=10m/s. The wall temperatures are 800K.

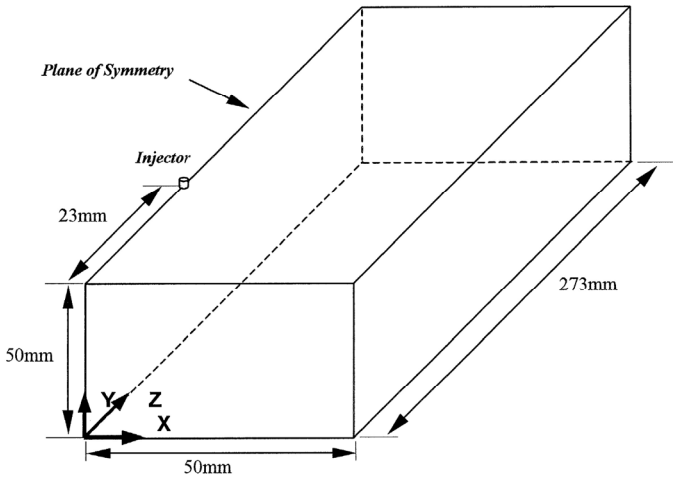

Fig. 1. Flow configuration

3. Results

To assess the computational method two sources of experimental data were used for the case of a polydisperse spray with a co-axial flow at atmospheric pressure (Heitor & Moreira, 1994) or elevated pressures (Barros, 1997). The method yielded reasonable results and revealed capabilities to improve the knowledge of the particle dispersion phenomena in more complex configurations. An example of the results obtained is shown in Figure 2, and a more complete analysis can be found in previous publications (Barata et al., 1999; Barata & Silva, 2000). The method was then extended to the case of an evaporating spray in a crossflow, and the evaporation models used by Chen and Pereira (1992) and Sommerfeld (1998) were tested and compared with the present model (see Barata, 2005 for details).

Figure 3 presents a parallel projection of the droplet trajectories in the vertical plane of symmetry (X=0) for two volatile fuels: n-Heptane and Ethanol. The former is used to define the zero limit of the anti-knock (resistance to pre-ignition) quality of fuels, while the other can be used to increase the octane number of gasoline. The higher volatility level of Ethanol can be inferred from Fig.3b) by the more uniform distribution at the right side of the domain and the trajectories in the direction of the top wall (at Y=0.05m). Due to the high volatility level of both fuels the droplets are injected and start almost immediately to evaporate, which gives rise to smaller droplets that follow quite closely the gaseous flow. Further downstream of the injection point, the trajectories of the droplets of Ethanol are more directed downwards than those of n-Heptane due to the higher fuel density and higher latent heat of vaporization. As a consequence, although a colder region near the injector is observed with Ethanol, the domain shows in general a much more uniform temperature distribution.

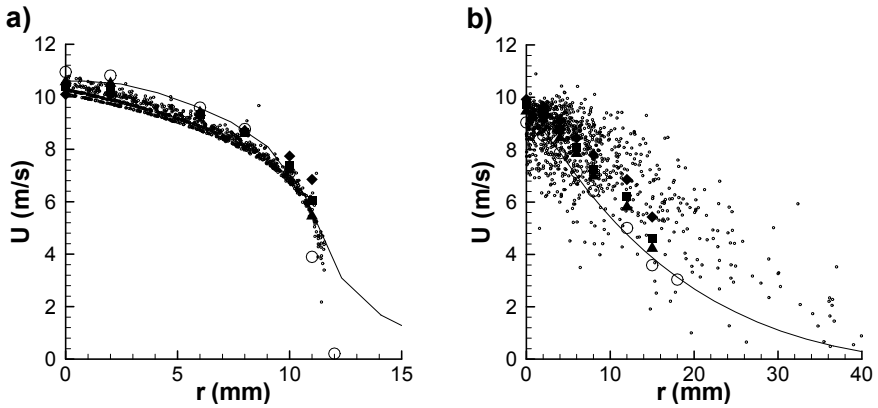

Fig. 2. Radial profiles of the mean axial velocity, *U*, at X/D=0.2 (a), and 6.5 (b). Experiments (Heitor & Moreira, 1994): ● , 30-35μm; ■ , 40-45μm; ♦ , 60-65μm; O, gaseous phase. Predictions: ° , particles; —— , gaseous phase.

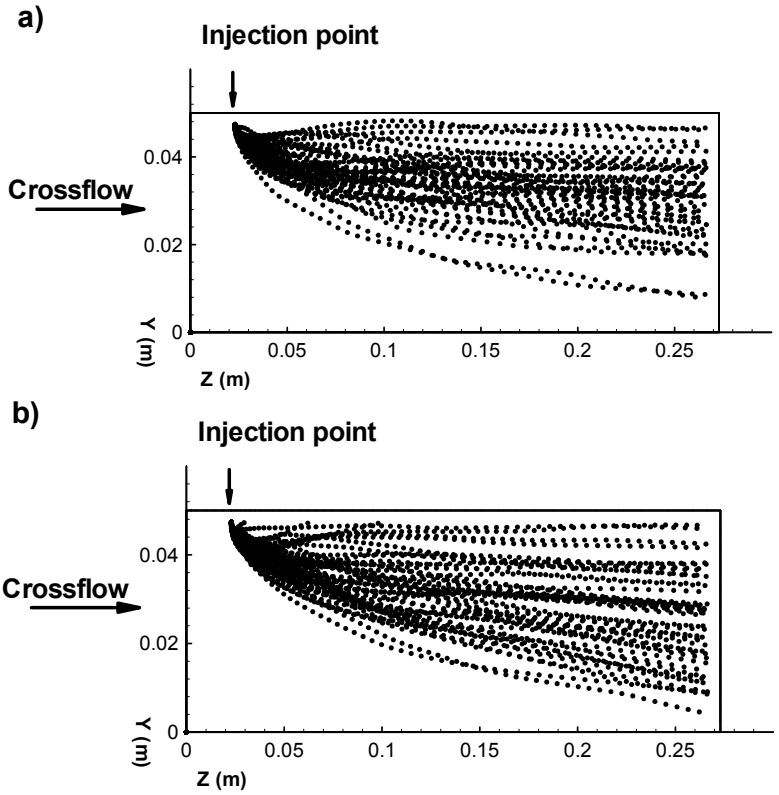

Fig. 3. Parallel projection of droplet trajectories in the vertical plane of symmetry (X=0) for W_{cross}=10m/s, V_p=-1m/s and T_p=293K: (a) n-Heptane; (b) Ethanol.

Figure 4 shows the droplet temperature and diameter variation time for the different fuels and test conditions used in the present work that are summarized in Table 5. The horizontal part of the line of the temperature variation with time (Fig.4a) reveals the equilibrium of the evaporation process that corresponds to the horizontal part of the droplet diameter variation with time. It should be pointed out that since the droplet is moving in the direction of the Z coordinate (with the crossflow), the ambient temperature may not be constant, and the evolution of the droplet diameter with time is also influenced by its velocity.

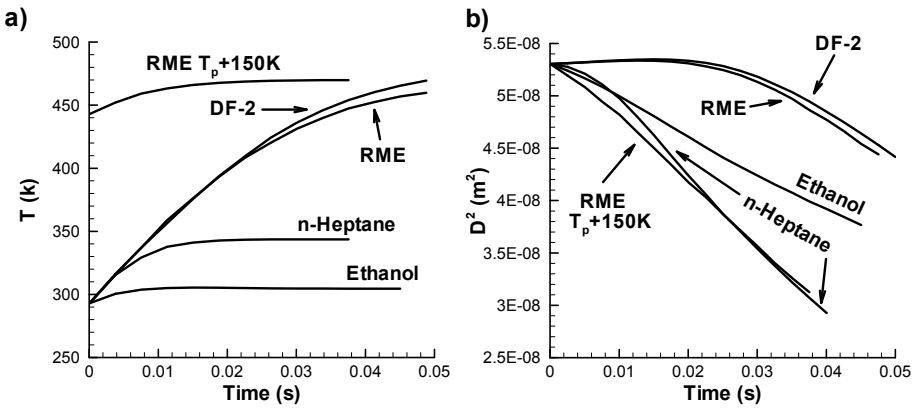

Fig. 4. Droplet temperature (a) and diameter (b) variation with time (W_{cross}=10m/s and V_p=-1m/s and T_p=293K).

The Rapeseed Methyl Ester (RME) and the Diesel Fuel (DF-2) have a higher boiling temperature and do not attain the equilibrium temperature in the first 50miliseconds (Fig.5a). As a consequence of the "pre-heating period" (about 20miliseconds in Fig.4b) the droplets diameters remain approximately constant and the evaporation starts later (Fig.4b).

Figure 5 shows parallel projections of the droplet trajectories in the vertical plane of symmetry, and confirms the main evaporation characteristics of the DF-2 and RME described in the previous paragraph. The pattern is similar for DF-2 and RME, although in the latter case there is a higher concentration of droplets in the core of the deflected monosize spray. This result is consistent with the slightly poorer evaporation characteristics of the RME deducted from Fig.5, and taking into account the average time that a droplet takes to reach the right hand side of the domain (at Z=0.3m) it is expected that its diameter would be (in average) at the exit of the channel about 92.2% of the initial diameter. So, in general the diameters of the droplets will be larger with DF-2 and RME, and the dispersion will be more difficult, because the slip between the gaseous phase and the dispersed phase will be more pronounced. Some collisions with the bottom wall are observed, but were not taken into account in the present study, although this phenomena has been investigated and reported elsewhere (see Barata & Silva, 2005).

Increasing the injection temperature of RME improves the evaporation of the droplets, and a more uniform distribution is obtained (Fig.5c). As shown in Fig.4, to obtain the equilibrium stage of evaporation near the injection point a pre-heating of 150K is required, which will be particularly difficult to implement in most of the practical situations.

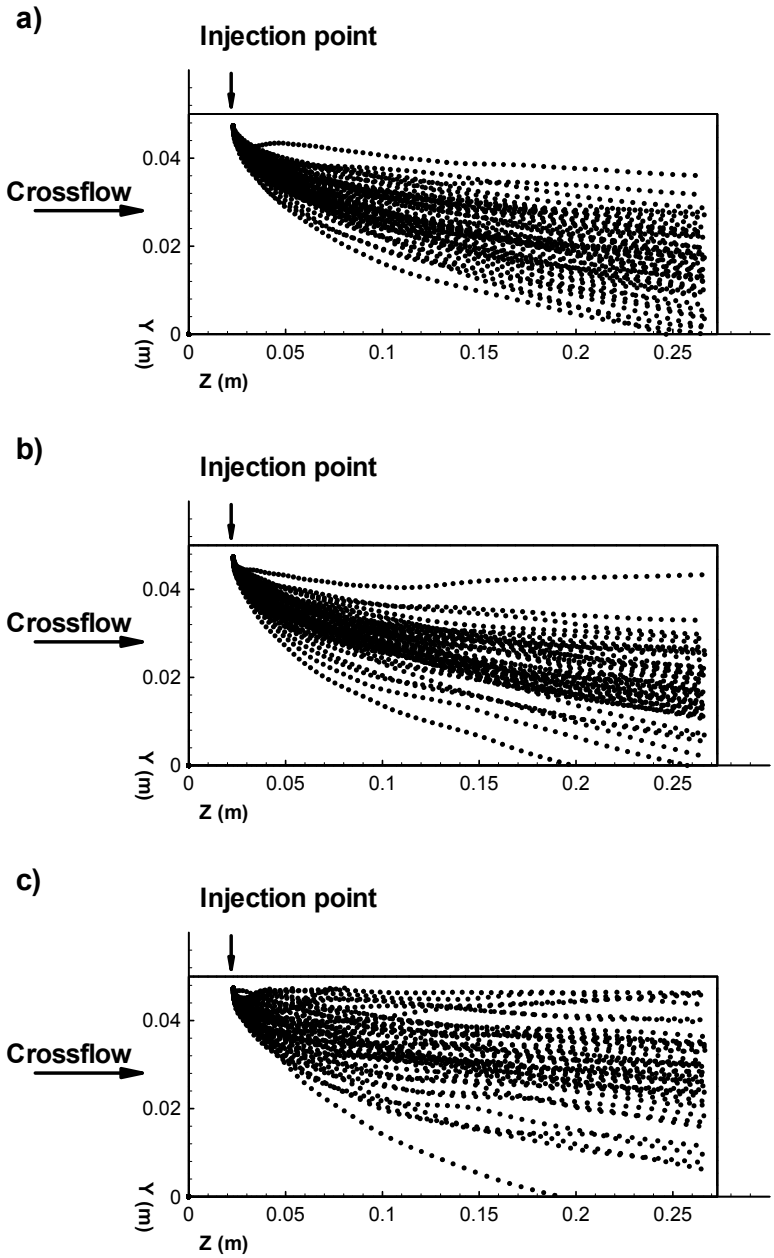

Fig. 5. Parallel projection of droplet trajectories in the vertical plane of symmetry (X=0) for W_{cross}=10m/s and V_p=-1m/s and T_p=293K.: (a) Diesel fuel (DF-2), T_p=293K; (b) RME, T_p=293K, (c) RME, T_p=443K.

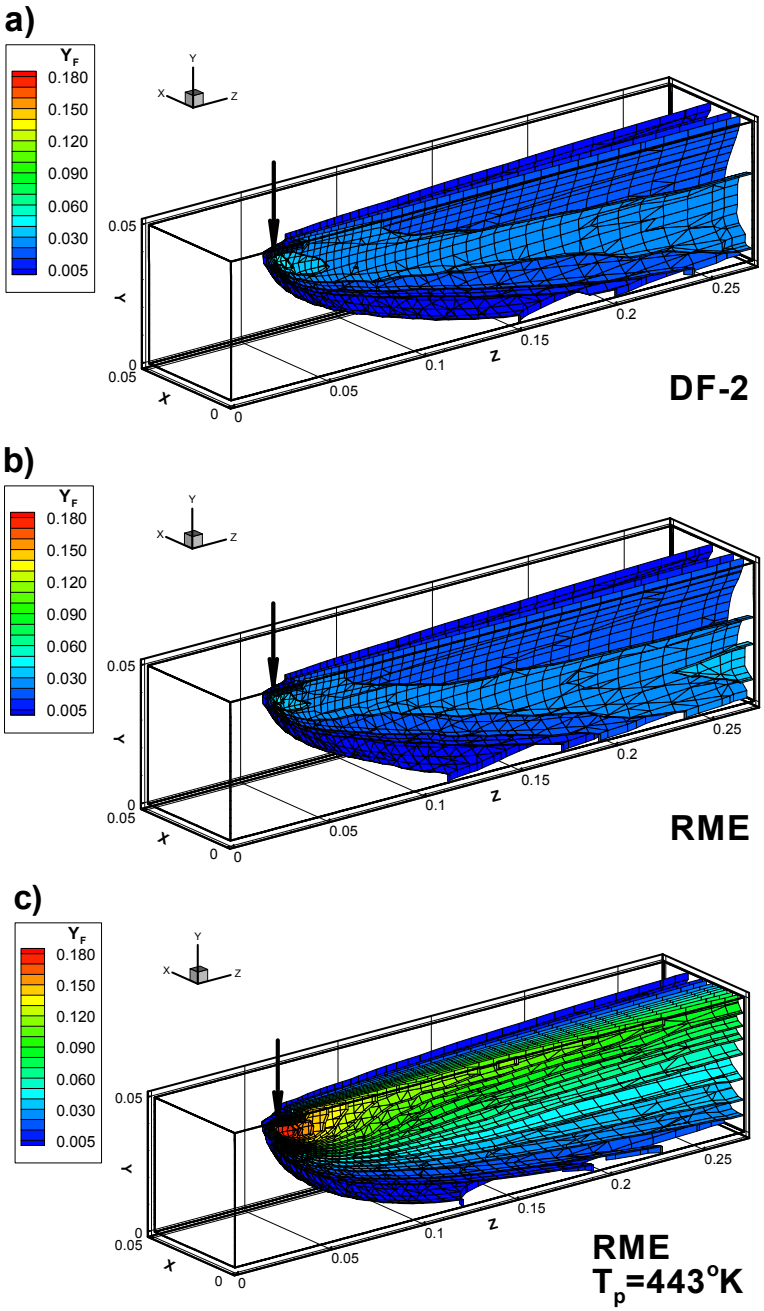

Fig. 6. Mass fraction distribution for W_{cross}=10m/s and V_p=-1m/s: (a) Diesel fuel (DF-2), T_p=293°K; (b) RME, T_p=293°K, (c) RME, T_p=443°K.

Fuel	n-Heptane	Rapeseed Methyl ester (RME)	Rapeseed Methyl ester (RME)	Diesel fuel (DF-2)	Ethanol
Droplets diameter, d	230,3μm	230,3μm	230,3μm	230,3μm	230,3μm
Crossflow velocity, $W_{crossflow}$	10m/s	10m/s	10m/s	10m/s	10m/s
Crossflow temperature, $T_{crossflow}$	800°K	800°K	800°K	800°K	800°K
Temperature of the walls, T_{walls}	800°K	800°K	800°K	800°K	800°K
Droplet injection velocity, V_p	-1 m/s	-1 m/s	-1 m/s	-1 m/s	-1 m/s
Droplet injection temperature, T_p	293°K	293°K	443°K	293°K	293°K
Ambient pressure	1 bar 101 350Pa	1 bar 101 350Pa	1 bar 101 350Pa	1 bar 101 350Pa	1 bar 101 350Pa
Mass loading	$20x10^{-4}$ Kg/s	$20x10^{-4}$ Kg/s	$20x10^{-4}$ Kg/s	$20x10^{-4}$ Kg/s	$20x10^{-4}$ Kg/s

Table 5. Summary of test conditions.

The evaporative characteristics of RME can be further analysed with the help of Fig.6 that shows a three-dimensional perspective of the mass fraction distribution with and without additional pre-heating. The results obtained with DF-2 and RME without additional pre-heating (Figs.6a and b) show that the mass fraction of fuel is always less than 0.04. For the DF-2 there is a larger evaporation near the injector, but further downstream the RME gives the higher values. When the additional pre-heating of 150K is used with RME, the domain shows a large region with a concentration of fuel vapour greater than 0.06, and the resulting pattern is quite similar to those obtained with more volatile fuels such as n-Heptane or Ethanol.

4. Conclusion

An Eulerian/Lagragian approach has been presented to calculate evaporating sprays through a crossflow. A method developed to study isothermal turbulent two- and three-dimensional dispersion was extended to the case of an array of evaporating biofuel droplets.

The droplet diameter, temperature and mass fraction distributions were found to be strongly dependent on the fuels used. Rapeseed Methyl Esters exhibit similar evaporating characteristics to DF-2, which indicates that it can be successfully used as an alternative fuel

in many applications that utilize diffusion flames. The use of RME in homogeneous combustion systems may require a prohibitive level of pre-heating, and the use of Ethanol (obtained from sugar or starch crops) may be a better alternative.

5. Aknowledgements

The present work has been performed in the scope of the activities of the AFTUR project. The financial support of the European Commission under Contract nº ENK5-CT-2002-00662 is gratefully acknowledged.

6. References

Abramzon, B. and Sirignano, W.A., Droplet Vaporization Model for Spray Combustion Calculations, *Int. J. Heat Mass Transfer*, vol.12, no.9, 1989, pp.1605-1648.

Arcoumanis, C., Whitelaw, D.S. and Whitelaw, J.S., "Gasoline Injection against Surfaces and Films, Atomization and Sprays, vol.7, pp.437-456, 1997.

Bai, C.X., Rusche, H. and Gosman, "Modeling of Gasoline Spray Impingement", *Atomization and Sprays*, vol.12, pp.1-27, 2002.

Barata, J.M.M., Lopes, P.N.S.D. and Perestrelo, N.F.F., "Numerical Simulation of Polydisperse Two-Phase Turbulent Jets". AIAA Paper 99-3760, 30th AIAA Fluid Dynamics Conference, Norfolk, VA, 28 June-1 July, 1999.

Barata, J.M.M. and Silva, A.R.R., "Numerical Study of Spray Dispersion in a Premixing Chamber for Low-NOx Engines". Millennium International Symposium on Thermal and Fluid Sciences, Xi'an, China, 18-22 September, 2000.

Barata, J.M.M. and Silva, A.R.R., "The Impingement of a Deflected Spray". Eighth International Conference on Energy for a Clean Environment, Lisbon, Portugal, 27-30 June, 2005.

Barros, A., "Projecto e Construção de um Labotatório de Atomização a Alta Pressão", MSc Thesis, *Instituto Superior Técnico*, Lisbon, December, 1997.

Berlemont, A., Grancher, M.S. and Gouebet, G., Heat and Mass Transfer Coupling Between Vaporizing Droplets and Turbulence Using a Lagrangian Approach, *Int. J. Heat and Mass Transfer*, vol.38, no.17, 1995, pp.3023-3034.

Chen, X.Q., and Pereira, J.C.F., "Numerical Prediction of Nonevaporating and Evaporating Fuels Sprays Under Nonreactive Conditions", *Atomization and Sprays*, Vol.2, 1992, pp.427-443.

Faeth, G. M., "Current Status of Droplet and Liquid Combustion", *Prog. Energy Combust. Sci.*, Vol. 3, 1977, pp. 191-224.

Faeth, G. M., "Evaporation and Combustion of Sprays", *Prog. Energy Combust. Sci.*, vol. 9, 1983, pp. 1-76.

Faeth, G. M., "Mixing, Transport and Combustion in Sprays", *Prog. Energy Combust. Sci.*, vol. 13, 1987, pp. 293-345.

Faeth, G. M., "Spray Combustion Phenomena", Twenty-Sixth Symposium (International) on Combustion/The Combustion Institute, 1996/pp. 1593-1612.

Godsave, G. A. E., "Studies of the Combustion of Drops in a Fuel Spray-the Burning of Single Drops of Fuel, Fourth Symposium (international) on Combustion". Williams & Wilkins, Baltimore, 1953, pp. 818-830.

Gosman, A.D. and Ioannides, E., "Aspects of Computer Simulation of Liquid-Fueled Combustors", AIAA Paper No.81-0323, *AIAA 19th Aerospace Sciences Meeting*, St. Louis, MO, 1981.

Heitor, M. V. and Moreira, A. L. N., "Experiments on Polydisperse Two-Phase Turbulent Jets", ICLASS-94, Rouen, France, Paper XI-5, July 1994.

Hubbard, G.L., Denny, V.E., and Mills, A.F., *Int. J. Heat Mass Transfer*, Vol.16, 1973, pp.1003-1008.

Launder, B.E. and Spalding, D.B., "The Numerical Computation of Turbulent Flows", *Computer Methods in Applied Mechanics and Engineering*, vol. 3, 1974, pp. 269-289.

Law, C. K., "Recent Advances in Droplet Vaporization and Combustion", *Prog. Energy Combust. Sci.*, Vol. 8, 1982, pp. 171-201.

Lefebvre, A. H., "Atomization and Sprays", Hemisphere Pub. Co., New York, 1989.

Leonard, B.P., "A Stable and Accurate Convective Modeling Procedure Based on Quadratic Upstream Interpolation", Computer *Methods in Applied Mechanics and Engineering*, vol. 19, No. 1, 1979, pp. 59-98.

Lockwood, F.C. and Naguib, A.S., "The Prediction of the Fluctuations in the Properties of Free, Round Jet, Turbulent, Diffusion Flames", *Combustion and Flame*, Vol.24, February 1975, pp.109-124.

Ranz, W.E. and Marshall, W.R. Jr., "Evaporation from Drops", *Chem. Eng. Prog.*, Vol.48, 1952, pp. 141-173.

Shirolkar, J. S., Coimbra, C. F. M. and Queiroz McQuay, M., "Fundamentals Aspects of Modeling Turbulent Particle Dispersion in Dilute Flows", *Prog. Energy Combusti. Sci.*, Vol. 22, 1996, pp. 363-399.

Shuen, J.S., Chen, L.D. and Faeth, G.M., "Evaluation of a Stochastic Model of Particle Dispersion in a Turbulent Round Jet", *AIChE Journal*, Vol.19, Jan. 1983, pp.167-170.

Shuen, J.S., Solomon, A.S.P., Zhang, Q.F., and Faeth, G.M., "Structure of a Particle-Laden Jets: Measurements and Predictions", *AIAA Journal*, Vol.23, No.3, pp. 396-404, 1985.

Sirignano, W. A., "Theory of Multi-component Fuel Droplet Vaporization" , *Archives of Thermodynamics and Combustion*, Vol. 9, No.2, 1978, pp. 231-247.

Sommerfeld, M., "Analysis of Isothermal and Evaporating Sprays by Phase-Doppler Anemometry and Numerical Calculations", *Int. J. Heat and Fluid Flow*, Vol.19, 1998, pp.173-186.

Spalding, D. B., "The Combustion of Liquid Fuels, Fourth Symposium (international) on Combustion". Williams & Wilkins, Baltimore, 1953, pp. 847-864.

Saparrow, E.M., and Gregg, J.L., *Trans. ASME*, Vol.80, 1958, pp.879-886.

Tinaut, F.V. (2005). "Performance of Vegetable Derived Fuels in Diesel Engine Vehicles", *Silniki Spanilowe*, No.2/2005 (121).

Watson, K.M., "Prediction of Critical Temperatures and Heats of Vaporization", *Ind. Eng. Chem.*, Vol.23, No.4, 1931, pp.360-364.

Williams, A., "Combustion of Droplets of Liquid Fuels, A Review", *Combustion and Flame*, Vol.21, 1973, pp1-31.

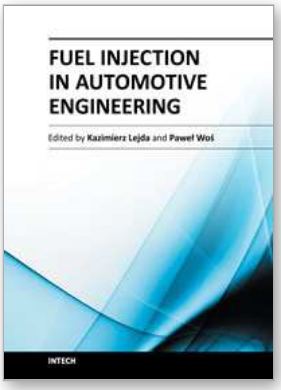

Fuel Injection in Automotive Engineering

Edited by Prof Kazimierz Lejda

ISBN 978-953-51-0528-2
Hard cover, 144 pages
Publisher InTech
Published online 20, April, 2012
Published in print edition April, 2012

The main topic of "Fuel injection in automotive engineering" book is fundamental process that determines the development of internal combustion engines and performances of automotive vehicles. The book collects original works focused on up-to-date issues relevant to improving injection phenomena per se and injection systems as the engine key components.

How to reference

In order to correctly reference this scholarly work, feel free to copy and paste the following:

Jorge Barata and André Silva (2012). Numerical Simulation of Biofuels Injection, Fuel Injection in Automotive Engineering, Prof Kazimierz Lejda (Ed.), ISBN: 978-953-51-0528-2, InTech, Available from: http://www.intechopen.com/books/fuel-injection-in-automotive-engineering/biofuels-injection

INTECH
open science | open minds

InTech Europe
University Campus STeP Ri
Slavka Krautzeka 83/A
51000 Rijeka, Croatia
Phone: +385 (51) 770 447
Fax: +385 (51) 686 166
www.intechopen.com

InTech China
Unit 405, Office Block, Hotel Equatorial Shanghai
No.65, Yan An Road (West), Shanghai, 200040, China
中国上海市延安西路65号上海国际贵都大饭店办公楼405单元
Phone: +86-21-62489820
Fax: +86-21-62489821